Check for
updates

Structural, conductivity, mechanical and wettability properties of copper alumina reinforced chlorinated polyethylene/polyvinyl chloride blend nanocomposites

S. Suvarna[1] · Furhan[1] · M. T. Ramesan[1]

Abstract

Copper alumina ($Cu–Al_2O_3$) has the greatest capacity to impart mechanical characteristics, crystallinity, thermal properties, conductivity and dielectric constant to a polymer matrix. This article presents the results of chlorinated polyethylene (CPE)/poly(vinyl chloride) (PVC) blend nanocomposites with different contents of nano-$Cu–Al_2O_3$. The presence of $Cu–Al_2O_3$ in the macromolecular chains of CPE/PVC blend was verified by FTIR spectra. SEM analysis showed the presence of hemispherical particles with nanometric sizes, and the XRD diffractograms revealed the crystalline peaks of $Cu–Al_2O_3$ in the blend nanocomposites. DSC studies revealed that the glass transition temperature of the blend shifted toward a higher value by the incorporation of $Cu–Al_2O_3$. An investigation of the electrical properties of blend nanocomposites demonstrates the enhancement in conductivity and dielectric nature with the addition of nanofillers. The effect of nanoparticles on different mechanical properties was also investigated. The modulus, tensile strength, hardness and impact properties of the blend nanocomposites were greatly enhanced, whereas the elongation at break decreased with the addition of nanofillers. Different tensile models were correlated with the experimental tensile values to study the mechanism of the reinforcement in blend matrix. Contact angle measurements of blend nanocomposites revealed that the addition of $Cu–Al_2O_3$ increased the hydrophobicity of the blend.

✉ M. T. Ramesan
mtramesan@uoc.ac.in

1 Department of Chemistry, Centre for Polymer Science and Technology, University of Calicut, Calicut University P.O., Kerala 673635, India

✆ Springer

Introduction

Polymer blending has become very common due to the low-cost method of producing polymeric materials with a wide range of commercial applications [1]. The most common interactions in polymer blends are hydrogen bonding, dipole–dipole interactions, ionic interactions and so on. The molecular interactions in polymers can be studied using a variety of methods, including spectroscopic techniques [2]. A higher degree of compatibility may result in increased phase stability and dispersed particle size [3]. These blends are found to have better properties than the individual component polymers. The blending of thermoplastic polymers gives new materials with excellent properties and some exceptions that are not exhibited by their pure polymers [4].

Polyvinyl chloride is a well-known polymer with exceptional properties in a wide range of applications. PVC is used in many different industries, including construction, irrigation, stationery, medical devices, electrical and automotive [5–7]. Other polymers with comparable properties can be blended with PVC to improve the mechanical strength, durability, resistance to oil and chemicals [8]. CPE thermoplastic resins are widely used in toughening properties of polymer matrix and have been shown to improve resistance to light, oxidizing agents and adhesive properties [9, 10]. CPE with varying Cl contents has an impact on the morphology and thermal stability of the resulting blends [11]. Studies on the effect of CPE on the mechanical properties of PVC have revealed increased impact strength and flexibility across a wide temperature range [12].

Polymer nanocomposites have recently sparked tremendous interest due to their low-cost and high-performance potential for a wide range of applications in automotive, aerospace, building construction, packaging, pharmaceuticals, medical devices and other industries. More intriguingly, their physical, mechanical, thermal and other properties can be tailored, opening up new technological and economic possibilities [13, 14]. Nanofillers are commonly used as reinforcing fillers in polymer matrix to improve the toughness, flame retardancy and mechanical properties [13, 15, 16]. Better dispersion and physical properties can be achieved by lowering the surface energy of these nanoparticles. Metal oxide nanocomposite has drawn wide attention due to its enhanced dielectric, thermal and mechanical properties. Oxides of transition metals are commonly used as fillers in various polymer products to achieve desirable characteristics [17, 18]. Cu nanoparticles are better in a variety of applications [18–20]. Good thermal properties, oil and chemical resistance, abrasion resistance, durability, etc., are some of the characteristics of its exceptional quality [21–25]. However, the inadequate mechanical properties of copper have to be addressed properly. The dispersion of nano-sized alumina into copper is an effective method to increase the mechanical strength, conductivity, dielectric properties and corrosion resistance of copper [26, 27]. The tribological behavior of alumina-coated metal nanocomposites was reported by Najjar et al. [28].

The addition of nanofillers to polymeric blend contributed to products that are lighter, stronger and less expensive materials in science and engineering

applications [29]. Polymer nanocomposites have different chemistry and properties than conventional polymer composites because nanometer-sized materials have an extremely high surface area that interacts with the polymer matrix at the molecular level [30]. There is no research available on the mechanical and dielectric properties of Cu–Al$_2$O$_3$/CPE/PVC blend nanocomposites. This work focuses on the structural, crystalline, morphological, electrical conductivity (at room temperature), wettability and mechanical properties of CPE/PVC blend with different contents of Cu-Al$_2$O$_3$ nanoparticles. Several theoretical modeling studies are carried out in order to corroborate the experimental tensile strength.

Experimental

Materials and methods

Polyvinylchloride with an average molecular weight of 60,000 g/mol was supplied by Sigma-Aldrich. Chlorinated polyethylene with 35% Cl content and a density of 1.213 gcm^{-3} was obtained from Alfa Aesar, India. Copper nitrate, aluminum nitrate, urea, tetrahydrofuran (THF) and toluene were purchased from Merck, India.

Preparation of CPE/PVC blend

The blend ratio of CPE and PVC was kept constant at 50:50, and it was prepared by dissolving 10 g of each polymer separately in THF and toluene as solvents and stirring continuously for 2 h until homogeneous liquids were formed. The CPE and PVC solutions were mixed with continuous stirring for 30 min. The polymeric blend solution was cast into glass plates and dried to get a constant blend film.

Synthesis of Cu-Al$_2$O$_3$ nanoparticles

The sol–gel technique [13] was used to make nanosized copper alumina powder by combining urea, copper nitrate and aluminum nitrate (in the ratio of 1:2:3) in an aqueous solution and stirring it with a magnetic stirrer at 100 °C. The gel form was then combusted in a muffle furnace at a temperature of 500 °C for 3 h. The powder obtained was kept in a desiccator.

Preparation of CPE/PVC /Cu-Al$_2$O$_3$ blend nanocomposites

The polymer blend nanocomposites were prepared by dispersing different contents of copper alumina nanoparticles (3, 5, 7 and 10 wt.%) with 50:50 ratios of CPE/PVC homogenous solutions as shown in Fig. 1. The mixture was stirred at room temperature and then ultrasonicated to obtain a clear solution. The CPE/PVC blend solution was then transferred into glass plates and set aside in a hot air oven at 50 °C for 48 h to obtain blend nanocomposite films. Here we use the
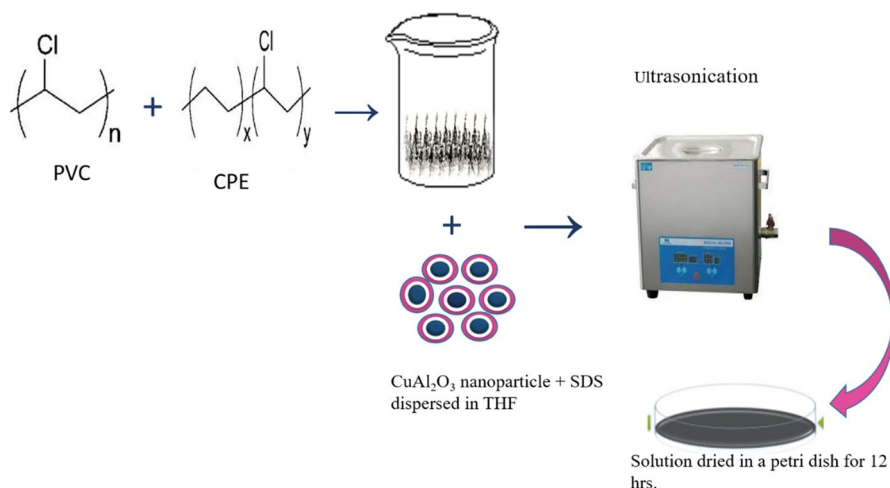
Fig. 1 Schematic illustration of CPE/PVC/Cu–Al$_2$O$_3$ blend nanocomposites

following sample code, B$_0$ is CPE/PVC blend without filler, and B$_3$, B$_5$, B$_7$, and B$_{10}$ are blend nanocomposites with 3, 5, 7 and 10 wt.% of copper alumina nanoparticles, respectively.

Characterization of blend nanocomposites

The FTIR spectroscopy in a range of 4000–400 cm^{-1} of Cu–Al$_2$O$_3$ nanoparticles and Cu–Al$_2$O$_3$ dispersed CPE/PVC blend was tested using a JASCO FTIR spectrometer to study structural facts of the polymeric material and interaction of functional groups. The Bruker D8 Advanced Diffractometer was used to study the XRD of the CPE/PVC blend and its composites with CuKα radiations at a scanning rate of 2º/min. Surface characteristics of the polymer blend and its nanocomposites were analyzed using scanning electron microscopy (SEM) with energy-dispersive X-ray spectroscopy (EDX) (FEI- NOVA NANOSEM-430). A differential scanning calorimeter was used to determine the glass transition temperature of the blend nanocomposites at a heating rate of 10 °C per min. The electrical characteristics of the composites were investigated using a programmed automated Hioki 3570 Model impedance analyzer. AC conductivity and dielectric constant were measured at various frequencies. The prepared blend nanocomposites were cut into dumbbell-shaped test specimens according to ASTM D638-08 for analyzing the mechanical properties. The tests were performed at room temperature in an Instron 3365 Universal Testing Machine with a cross-head speed of 500 mm min^{-1}. The notched Izod impact test as per ASTM D256 was carried out using the ZWICK 5102 impact-testing machine. The hardness of molded blend and their composites was determined using a Shore D durometer.

Results and discussion

Fourier transform infrared spectroscopy

Structural analysis of the polymer blend and its nanocomposites is investigated using FTIR spectroscopy, and the results are given in Fig. 2. The peaks at 2946 cm^{-1} and 1392 cm^{-1} correspond to the C-H stretch and C–C stretch, respectively, in the backbone of CPE/PVC blend segments. The peak observed at 539 cm^{-1} indicates the C–Cl bond stretching. For composites, the C–Cl peak is slightly shifted to 677 cm^{-1}. Compared to the CPE/PVC blend, broadening can be observed for the C–H and C–C stretches in the blend nanocomposites and a slight shift for C–H stretch to 2964 cm^{-1} can be observed. The spectra of Cu–Al$_2$O$_3$ contain a peak at 470 cm^{-1} that corresponds to the O–Al–O stretching in copper alumina nanoparticles [31]. Broad and weak absorption bands appeared at 3697 cm^{-1} and 157 cm^{-1} due to the stretching and bending of O–H vibration on the nanoparticle surface. The band corresponding to O–Al–O stretch is shifted to 457 cm^{-1} and 465 cm^{-1} for 7 wt.% and 10 wt.% loadings of nanocomposites, respectively. Similarly, O–H vibration bands of nanofillers also shifted to a lower wavenumber, that is to 3440 cm^{-1} for 7 wt.% and 3432 cm^{-1} for 10 wt.% samples. The intensity of this peak corresponds to the Al-O stretch from the nanofiller, which is maximum at 7 wt.% of the nanocomposite. Beyond this, the intensity seems to be decreasing. This is due to the poor interfacial interaction of nanoparticles with the polymer blend. This circumstance results in a decline of vibrational transitional energy and, thereafter, a decrease in peak intensity.
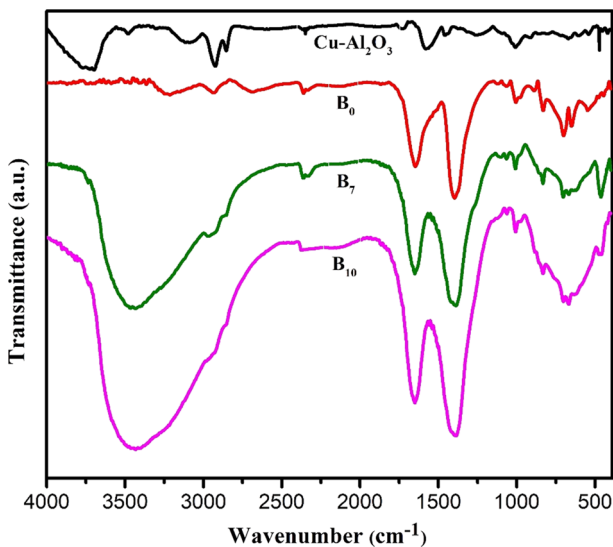

Fig. 2 FTIR spectrum of CPE/PVC blend with Cu–Al$_2$O$_3$ nanoparticles

X-ray diffraction analysis (XRD)

X-ray diffractometer is used to characterize the copper alumina-filled CPE/PVC blend, and the results are given in Fig. 3. The semi-crystalline nature of the CPE/PVC blend can be perceived by the four major peaks centered at $2\theta = 12.49$, 19.19, 25.19 and 28.85 degrees. The sharp peaks for $Cu–Al_2O_3$ illustrate its higher crystalline nature ($2\theta = 35.30$, 38.67, 43.7, 49.8, 57.63 and at 66.08 degrees). The loading of metal oxide nanoparticles into the polymer blend increases the crystallinity of the blend. The XRD peaks of the composites show major crystalline peaks of nanoparticles with a decrease in the broadness of the amorphous region of the polymer blend. There is a shift of 2θ angles for the polymer blend after the addition of nanofillers. For instance, one peak in the XRD band of a bare polymer blend at 2θ angle of 28.8 shifts to 20.2 degree for a 5 wt.% sample. The mean crystalline size (D) of $Cu–Al_2O_3$ nanoparticles is found to be ~ 26.8 nm using the Scherrer equation.

$$D = \frac{k\lambda}{\beta \cos\theta} \tag{1}$$

where $k = 0.89$, a constant called the shape factor, and β is the full width at half maximum of diffraction peaks (in radian) [32]. The average interchain separation can be determined using the below equation.
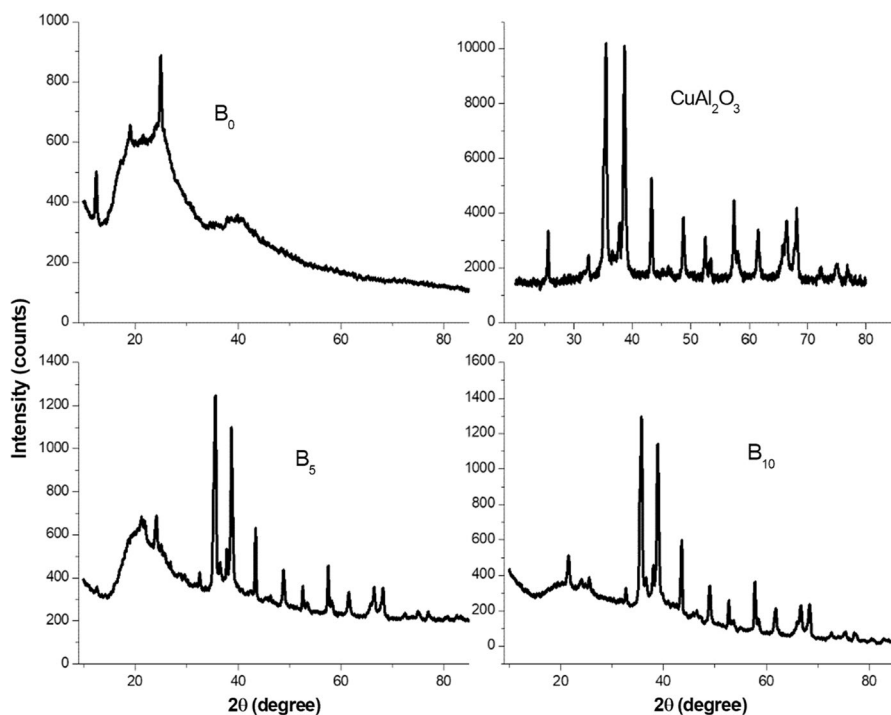

Fig. 3 X-ray diffraction pattern of CPE/PVC blend and its nanocomposites

$$s = \frac{5\lambda}{8\sin\theta} \tag{2}$$

where λ is the wavelength of the incident X-ray beam (1.54184 Å) and is the Bragg diffraction angle of the peak with maximum intensity [32]. The value of S is found to be nearly 2.29 Å. The interchain separation is reduced to 2.17 for 5 wt.% and 2.00 for 10 wt.%, indicating the effective interlinkage of nanoparticles within the polymer blend chain. These changes further manifest the successful incorporation of Cu–Al$_2$O$_3$ within the blend matrix.

Field emission scanning electron microscopy (FESEM)

FESEM is a potential method for visualizing filler distribution and dispersion, as well as their physical interactions with the polymer matrix. Figure 4 shows the FESEM analysis of the copper alumina filled CPE/PVC blend nanocomposites. The SEM image of the pure blend revealed a heterogeneous structure with voids distributed on the surfaces. However, incorporating Cu–Al$_2$O$_3$ into CPE/PVC composites created a smooth surface with the distribution of hemispherical fillers in the polymer matrix. This uniform morphology is owing to the rise in the number of polar–polar interactions between nanoparticles and blend segments, which confirms the possibility of enhancement of the mechanical properties of the films. The surface of the composite is getting more rough and jagged with higher loadings of nanoparticles
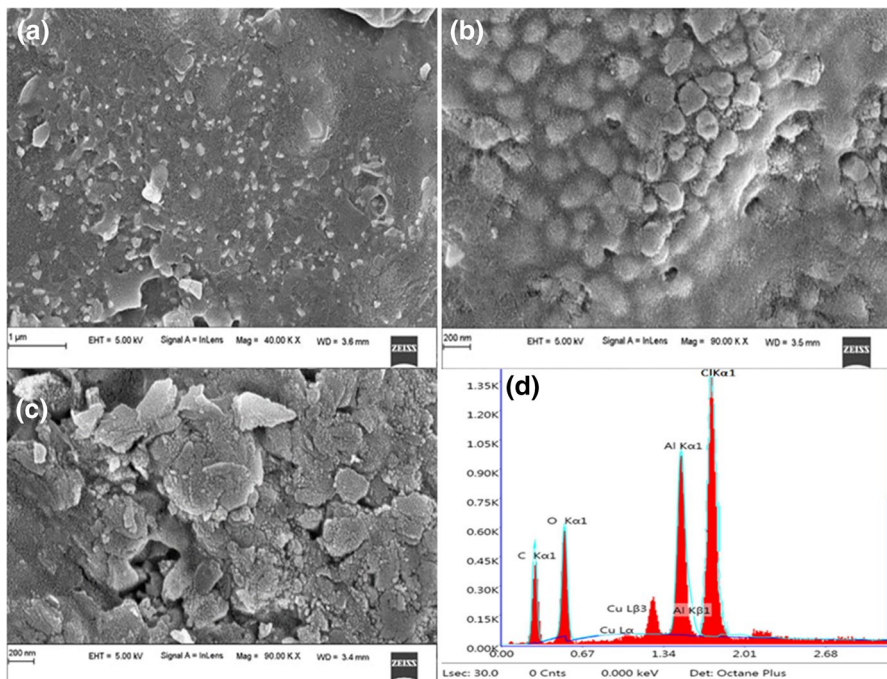

Fig. 4 FESEM images of **a** B$_0$ **b** B$_5$ and **c** B$_{10}$ and **d** EDX spectrum of B$_{10}$ blend nanocomposite

(10 wt.%). This non-uniform aberrant surface of the material is due to the poor interfacial interaction between the nanofillers and the polymer, which leads to an agglomeration of nanoparticles [33, 34]. The presence of C, O, Cu, Al and Cl elements in the EDX spectrum of blend nanocomposite indicates that Cu–Al_2O_3 nanoparticles are uniformly dispersed in the CPE/PVC blend (Fig. 4d).

Differential scanning calorimetry

The DSC offers qualitative and quantitative information on endothermic and exothermic processes. A constant change in the slope of the heat flow *Vs* temperature profile, together with a matching change in the material's heat capacity, characterizes the glass transition. The DSC studies of the CPE/PVC blend and its composite with copper alumina nanoparticles of various loadings are illustrated in Fig. 5. It is found that the glass transition temperature (T_g) of CPE/PVC blend is obtained at 72.43 ^{0}C and the single T_g indicates the compatibility between the two polymer segments. The heat flow through the sample becomes more efficient with the inclusion of nanofillers, where the segmental mobility of polymer chains becomes more restricted and thus the glass transition temperature of the composites increases slightly with the filler addition. The T_g values are 76.21 °C and 80.28 °C for 5% and 10% loadings, respectively. The melting point T_m of the bare blend is 130.2 °C from the sharp endothermic peak of the plot, whereas, for 5 wt.% and 10 wt.% samples, the melting point increased to 134.28 and 138.19 °C, respectively. The interlinkage of nanoclusters within the polymer chain causes the material to become more rigid through the hindrance made to the chain segments, and this is the cause of an increase in the glass transition [35] and melting temperature of the composites. Moreover, the regular structure attained by the macromolecular chain due to uniform adsorption of monomer molecules on Cu–Al_2O_3 nanoparticle surface makes the material less flexible and thereby
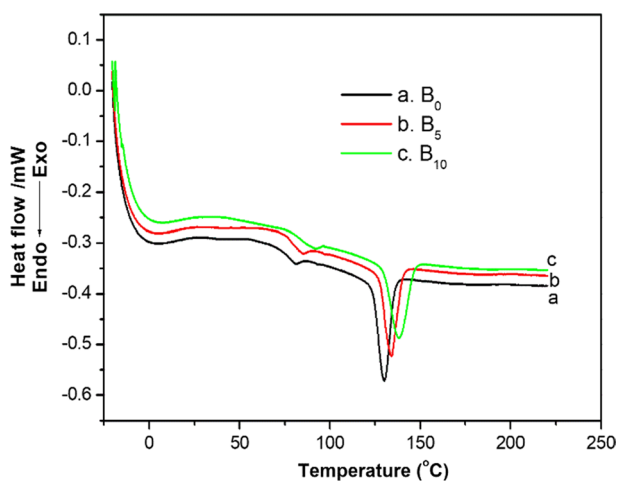

Fig. 5 DSC curves of CPE/PVC blend with different contents of Cu–Al_2O_3

leads to enhanced T_g values. The shift in T_g values further confirms the successful reinforcement of crystalline Cu–Al_2O_3 nanoparticles into the polymer blend segments.

AC conductivity

The variation in AC conductivity with frequencies of CPE/PVC blend and its copper alumina nanocomposites at different loadings is shown in Fig. 6. The conductivity of all samples increases with frequency. The inclusion of copper alumina nanoparticles develops more charge carriers, and their mobility results in higher conductivity. The enhanced conducting nature of all the nanocomposites at higher frequencies is attributed to the hopping mechanism of charge carriers [36]. The maximum conductivity is exhibited by 7 wt.% loaded sample that can be correlated with the uniform arrangement of the nanoparticles within the polymer matrix. In addition, the effective conducting network formation of charge carriers in this sample also contributes to enhanced conductivity. However, a slight decrease in conductivity is observed at higher loadings due to the inhomogeneous distribution of nanoparticles that hinder the movement of charge carriers [37].

The AC conductivity can be mathematically expressed in terms of applied field and permittivity as follows,

$$\sigma_{ac} = \omega \varepsilon_0 \varepsilon'' \tag{3}$$

here ε_0 is the permittivity of free space and ε'' is the product of dielectric constant ε' and dielectric loss tan δ [38].
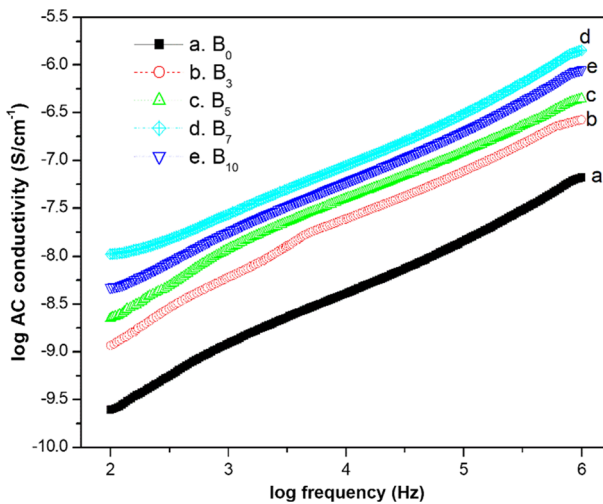

Fig. 6 AC conductivity of CPE/PVC blend and its nanocomposites

Dielectric constant

The dielectric constant of a material is its ability to retain electrical charge, and it is calculated as the ratio of the relative permittivity to the free space permittivity. Charges build in the heterogeneous interphase of the material with varied permittivity and conductivity when an electric field is applied, as explained by the Maxwell–Wagner effect [39, 40]. The variation in dielectric constant with frequency for the CPE/PVC blend and its Cu–Al_2O_3 nanocomposites is shown in Fig. 7. The higher value of the real part of permittivity at smaller frequencies is due to the accumulation of charges at the grain boundaries, resulting in the formation of a potential barrier [41]. It can be seen that the dielectric value decreases with a frequency up to 10^3 Hz. This abating trend in dielectric constant is attributed to the reduction in space charge polarization. At higher-frequency domains, the dielectric constants become frequency independent due to the dielectric relaxation mechanism, which is the inability to gain the energy needed to orient the oscillating field with the applied frequency [42, 43]. The maximum dielectric constant is exhibited by 7 wt.% of the sample, after that a significant decline in value can be observed, which is ascribed to the agglomerating nature of nanoparticles that leads to poor intermolecular interaction, thereby reducing the contribution to the charge storage.

Mechanical properties

Table 1 shows the mechanical parameters such as Young's modulus, tensile strength, elongation at break, hardness and impact strength of CPE/PVC/Cu–Al_2O_3 nanocomposites. Lower tensile strength, modulus and higher elongation at break of a bare polymer blend indicate poor mechanical strength. However, the inclusion of Cu–Al_2O_3 nanofillers enhances the tensile strength of the polymer
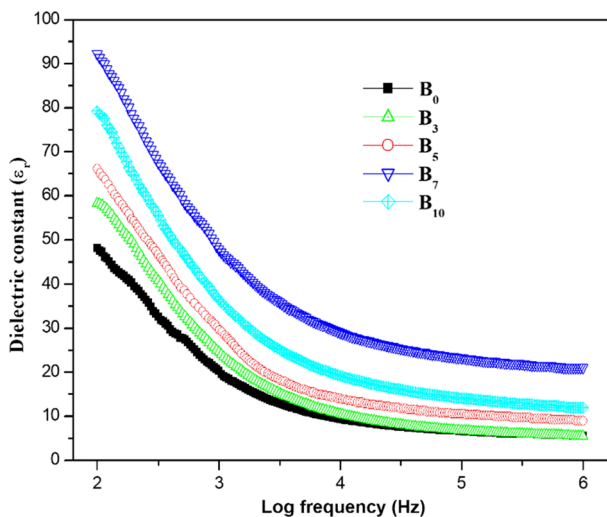

Fig. 7 Dielectric constant CPE/PVC blend with different contents of Cu–Al_2O_3

Table 1 Mechanical properties of CPE/PVC blend and its nanocomposites

Sample loadings	Young's modulus	Tensile strength (MPa)	Elongation at break (%)	Hardness (Shore D)	Impact strength (J/m)
0	1.01 ± 0.28	21 ± 0.53	88 ±2	44 ± 0.54	11 ± 0.62
3	1.15 ± 0.24	26 ± 0.49	82 ±3	45 ± 0.48	13 ± 0.68
5	1.29 ± 0.22	32 ± 0.45	77 ±1	47 ± 0.52	16 ± 0.59
7	1.43 ± 0.28	38 ± 0.51	73 ±2	49 ± 0.51	18 ± 0.61
10	1.39 ± 0.25	35 ± 0.52	70 ±3	51 ± 0.49	17 ± 0.62

blend and it seemed to be increasing with an increment in embedded filler quantity. The Young's modulus of a material is used to specify the compressive stiffness of a material under an elongation, quantifying the ratio of axial strain ε to the tensile/compressive stress σ. The Young's modulus of bare CPE/PVC blend is found to be 1.01 GPa, and for composites, the modulus increased with filler concentration. The maximum Young's modulus is obtained for 7 wt.% loadings (1.43 GPa). Beyond that, a slight decrease is observed and this is due to the non-uniform distribution and agglomeration of nanoparticles. It can be observed from the table that the tensile strength increases up to 7 wt.% of sample is due to the effective interfacial interaction of nanoparticles and blend matrix, facilitating the matrix-filler stress transfer [44]. The inadequate connectivity between the filler nanoparticle and the polymer chain due to the aggregating nature of the nanoparticles is ascribed to further losses in tensile strength with increasing filler loading. The impact strength of a material refers to how much energy it can endure when a load is applied quickly. The hardness and impact strength of the samples increase with the concentration of filler. The highest impact strength (18 J/m) is exhibited by 7 wt.% nanocomposites. Elongation at break is the ratio of change in length to the initial length after breakage of the sample [45] declines, and thus, the material is said to be of improved mechanical strength due to the restrictions imparted by the rigid nanofiller.

Tensile modeling

There are several theoretical methods for calculating tensile strength and connecting these results with actual data aids in determining the influence of nanofillers on the mechanical properties of polymer nanocomposites. These models take into account the connectivity of polymer chains and nanoparticles, as well as the influence of volume fractions of these fillers on mechanical strength. Most of these models are based on the volume fraction of nanofiller and the tensile strength of the polymer matrix. Some models additionally take into account the size parameters, crowding factor and dispersion index, among other things, and so provide insight into how these parameters affect the mechanical characteristics of polymer mix nanocomposites.

Kerner model

Kerner proposed a model to determine the tensile strength of nanocomposite M_c based on the volume fraction V_f, matrix tensile strength M_m and a parameter V_m relates to the interaction factor [46].

$$M_c = M_m \left[1 + \left(\frac{Vf\, 15(1-Vm)}{(1-V_f)(8-10Vm)} \right) \right] \qquad (4)$$

According to this concept, tensile strength Mc improves as the volume percent of the nanofiller increases. However, this model does not correlate with the experimental results and the resulting values are higher than the theoretical prediction. The obtained results from the experiment and theoretical equation are shown in Fig. 8. A maximum value of tensile strength at 7 wt.% sample is observed for experimental results, whereas the theoretical values do not show this percolation limit.

Einstein model

Einstein suggested a simple model based on the filler volume fraction and the tensile characteristics of the polymer matrix. The Einstein equation can be used to determine the tensile strength Mc of a blend nanocomposite [45]

$$M_c = M_m(1 + 2.5V_f) \qquad (5)$$

Similar to the experimental results, the theoretical values also exhibit an increasing trend with the rise in filler loading. The obtained result is plotted for theoretical and
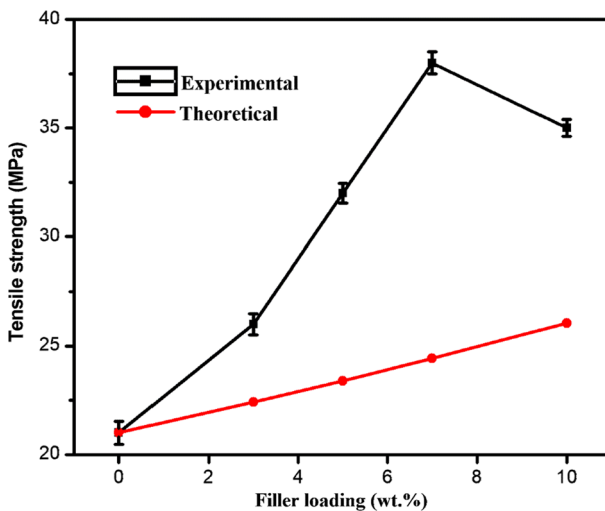

Fig. 8 Experimental and theoretical tensile strength of CPE/PVC/Cu–Al$_2$O$_3$ nanocomposites based on Kerner model

experimental calculation in Fig. 9. Theoretical values are lower than the experimental results, but the deviation is not much as that observed with the Kerner model.

Einstein model predicts that the tensile strength of a blend nanocomposite mostly depends on the volume fraction of filler loading and no other parameters are taken into consideration for the calculation. According to this hypothesis, as the volume percentage of nanoparticles increases, the tensile strength of the composite increases.

The tensile modulus of polymer nanocomposites has been extensively studied experimentally and computed using a two-phase model that includes matrix and filler. Einstein equation is one of the first theories for a nanocomposite system in a non-rigid matrix, and it is based on considering the viscosity of a suspension of spherical rigid particles. This equation seems to be applicable only for the low volume fraction of filler. By increasing the filler volume percentage, strain fields around filler particles start to interact [47]. These challenges related to the evaluation of interaction parameters led to the further development of other models proposed by Guth and Mooney.

Guth model

Guth suggested a theoretical model based on the Einstein equation for determining the tensile strength of blend nanocomposites, in which the Einstein equation is modified by adding a square parameter of volume percent as shown below [40, 47].

$$M_c = M_m\left(1 + 2.5V_f\right) + 14.1V_f^{\,2} \tag{6}$$

However, the equation does not give a result that agrees with the experimental findings. As a result, a thickness parameter d is added to the model to make it
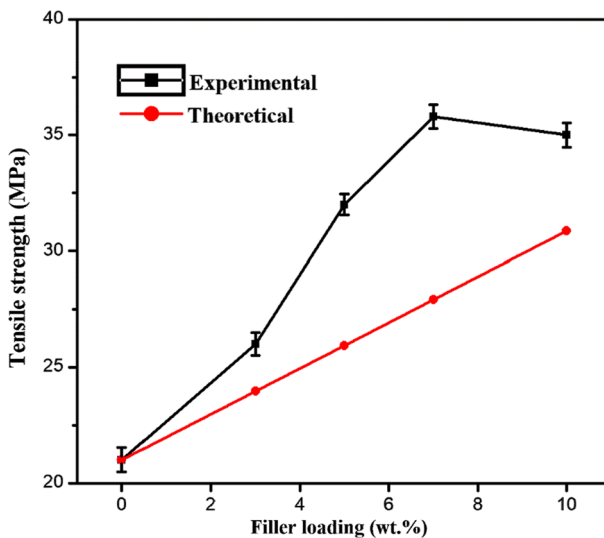

Fig. 9 Experimental and theoretical tensile strength of CPE/PVC/Cu–Al$_2$O$_3$ nanocomposites based on Einstein model

more consistent with experimental tensile strength, and the suggested equation is as follows,

Modified Guth model

$$M_c = M_m \left(1 + 2.5 V_f / d \right) + 14.1 V_f^2 \qquad (7)$$

The obtained result is plotted along with the experimental result given in Fig. 10.

The figure shows a better correlation between the experimental and theoretical strength of the material. Both have maximum tensile strength for 7 wt.% of the sample due to their effective filler-blend matrix interlinkage, and beyond that, there is a slight decrease in the tensile value at higher loading, which is attributed to the decline in interfacial linkage resulting in poor stress transfer within the material. This means that at higher nanoparticle contents, the aggregation of nanoparticles occurs in the blend matrix. Surface energy is high in nanoparticles with a large surface area to volume ratio. To lower their surface energy, nanoparticles cluster together. At this stage, the polymer matrix covers the agglomerated particles, reducing the rate of interphase volume growth. Tensile strength is reduced as a result of volume fraction expansion.

Mooney model

The Mooney model is a theoretical modification of the Einstein model that takes into account a parameter relating to the strain field around the two phases, filler and polymer matrix [46, 48]. The modified equation is shown below.
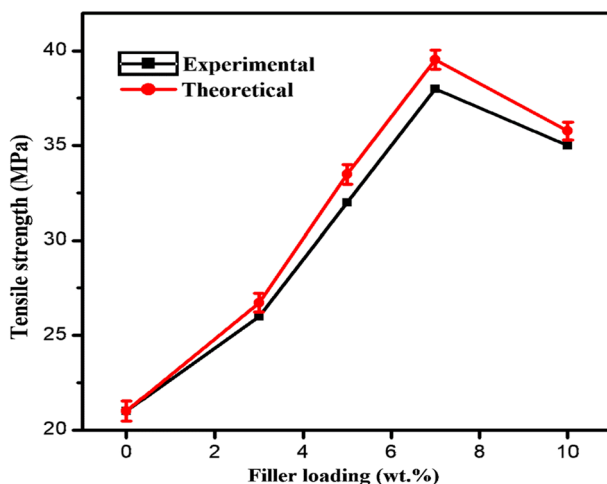

Fig. 10 Experimental and theoretical tensile strength of CPE/PVC/Cu–Al$_2$O$_3$ nanocomposites based on modified Guth model

$$M_c = M_m e^{\left(\frac{2.5V_f}{1-sV_f}\right)} \qquad (8)$$

This model is more commonly used to describe the non-elastic behavior of materials. The comparison of tensile strength based on Mooney model and experimental results is depicted in Fig. 11. The theoretical tensile strength is much lower than the experimental tensile values, indicating that this model fails to explain the reinforcement of Cu-Al$_2$O$_3$ nanoparticles within the CPE/PVC blend. Based on the Mooney model, only small volume fractions of the sample have equivalent actual and theoretical tensile strength.

Contact angle measurement

The surface hydrophobicity of a nanocomposite film and the influence of the filler on the conversion of a composite to hydrophobic or hydrophilic, as well as the state of dispersion of fillers can be examined via contact angle measurement. The contact angle of CPE/PVC blend and its Cu–Al$_2$O$_3$ nanocomposites of various loadings are measured, and the obtained results are depicted in Fig. 12. An increase in angle for each addition of filler indicates the hydrophobicity added to the material surface. Copper alumina interposed into the polymeric materials can be a potential approach to enhancing the surface roughness. It is clear that hydrophobic solids are often low-surface-energy solids that interact predominantly through dispersive interactions [49]. Water molecules form strong hydrogen bonds with one another. The partial loss of hydrogen bonding of water molecules in contact with a hydrophobic substance that does not undergo hydrogen bonding causes the area of contact to be minimized [50].
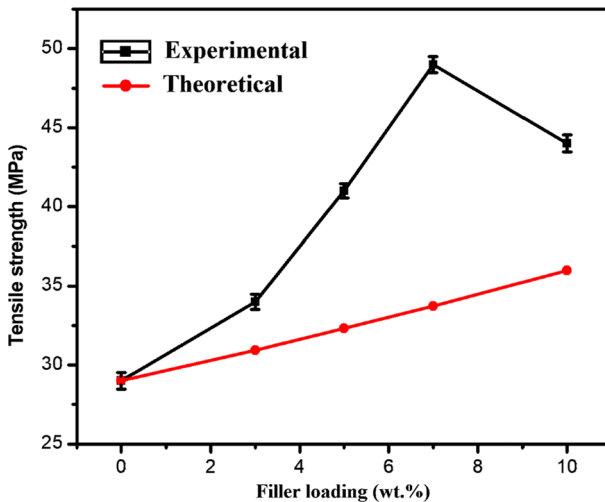

Fig. 11 Experimental and theoretical tensile strength of CPE/PVC/Cu–Al$_2$O$_3$ nanocomposites based on modified Mooney model
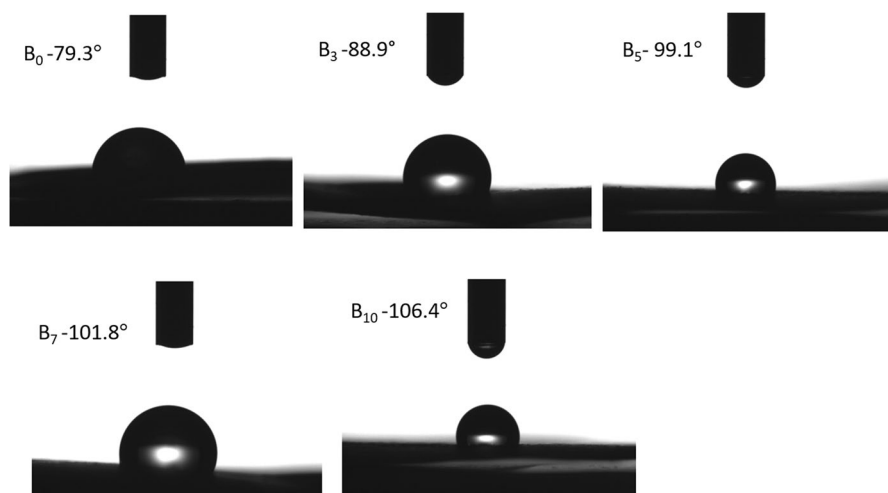
Fig. 12 Contact angle of CPE/PVC/Cu–Al$_2$O$_3$ nanocomposites

Conclusion

The Cu–Al$_2$O$_3$ nanoparticle reinforced CPE/PVC blend nanocomposites were successfully prepared by the solution method. Fourier transform IR spectroscopy revealed the formation of CPE/PVC/Cu–Al$_2$O$_3$ nanocomposite. The semicrystalline nature of the blend and crystallinity imparted by the nanofiller was confirmed by the XRD analysis. The dispersion of Cu–Al$_2$O$_3$ nanoparticles in the chlorinated CPE/PVC blend was confirmed by EDX analysis. DSC analysis revealed the increased physical transition temperature caused by the significant addition of nanofiller. The CPE/PVC/Cu–Al$_2$O$_3$ nanocomposites exhibit enhanced dielectric parameters and AC conductivity than pure polymer blend, and these properties increase up to 7 wt.% loadings and then decrease due to nanoparticle agglomerations within the polymer blend matrix. The mechanical properties, such as tensile strength, hardness, modulus and impact resistance of the blend nanocomposites, were improved significantly with the loading of nanoparticles, whereas the elongation at break decreased. Different theoretical models were compared with the experimental results and the Guth model based on the thickness parameter made the theoretical and experimental results show a good correlation. The contact angle measured for the CPE/PVC blend and its Cu–Al$_2$O$_3$ nanocomposites showed the improved hydrophobicity of the material. All these results revealed the enhancement in physical properties such as electrical and mechanical properties as well as the moisture resistance of the CPE/PVC blend through the inclusion of Cu–Al$_2$O$_3$ nanoparticles, and thereby, the CPE/PVC/Cu–Al$_2$O$_3$ polymer nanocomposites can be used in various optoelectronic and construction components.

Declarations

References

1. G. Zhu, F. Wang, K. Xu, S. Dong, Res. Chem. Intermed. **41**, 1097 (2015)
2. G. Zhu, F. Wang, Q. Gao, X. Kejing, L. Yuying, Res. Chem. Intermed. **40**, 1583 (2014)
3. A. Nihmath, M.T. Ramesan, Res. Chem. Intermed. **46**, 5049 (2020)
4. K. Parvathi, B.K. Bahuleyan, M.T. Ramesan, Res. Chem. Intermed. **48**, 3897 (2022)
5. A. Keivanloo, M. Bakherad, M. Khosrojerdi, A.H. Amin, Res. Chem. Intermed. **44**, 2571 (2018)
6. T. Zhang, J. Zhou, Y. Chen, Res. Chem. Intermed. **44**, 5329 (2018)
7. Y. Zhang, Z. Zhang, Y. Chen, Y. Li, Res. Chem. Intermed. **43**, 7307 (2017)
8. D. Garcia, R. Balart, J.E. Crespo, J. Appl. Polym. Sci. **101**, 2464 (2006)
9. Z. Zhang, J. Zhang, H. Liu, Polym. Eng. Sci. **54**, 378 (2013)
10. K. Marossy, P. Bárczy, Polym. Compos. **11**, 115 (2003)
11. Y.J. Shur, B. Ranby, J. Appl. Polym. Sci. **20**, 3105 (1976)
12. T. Wang, X. Li, Y. Xiong, Y. RSC Adv. **10**, 44584 (2020)
13. S. Sankar, M.T. Ramesan, J. Mat. Sci. Mat. Electron. **33**, 21762 (2022)
14. M.Z. Rong, M.Q. Zhang, W.H. Ruan, J. Mater. Sci. Technol. **22**, 787 (2006)
15. Furhan, M.T. Ramesan, Polym. Eng. Sci. **62**, 3418 (2022)
16. X. Yue, C. Li, Y. Ni, J. Mater. Sci. **54**, 13070 (2019)
17. T. Iqbal, M. Irfan, S.M. Ramay, J. Polym. Environ. **28**, 2422 (2020)
18. W. Wei, Z. Liu, J. Power Sources **238**, 376 (2013)
19. K. Giannousi, I. Avramidis, C.D. Samara, RSC Adv. **3**, 21743 (2013)
20. J. Ramyadevi, K. Jeyasubramanian, A. Marikani, Mater. Lett. **71**, 114 (2012)
21. S. Sankar, M.T. Ramesan, Polym. Eng. Sci. **62**, 2402 (2022)
22. N. Hussain, M. Mehdi, S.H. Siyal, J. Appl. Polym. Sci. **138**, 51381 (2021)
23. G. Qin, L. Fan, A. Watanabe, J. Mater. Sci. **50**, 49 (2015)
24. M.S.A. Elwahed, A.F. Ibrahim, M.M. Reda, J. Mater. Res. Technol. **9**, 8528 (2020)
25. A. Fathy, A. Shaker, M.A. Hamid, A.A. Megahed, J. Compos. Mater. **51**, 1667 (2017)
26. S. Sankar, A. George, M.T. Ramesan, RSC Adv. **12**, 17637 (2022)
27. S. Suvarna, Furhan, M.T. Ramesan, J. Indian Chem. Soc. **99**, 100772 (2022)
28. I.R. Najjar, A.M. Sadoun, A. Fathy, A.W. Abdallah, M.A. Elaziz, M. Elmahdy, Lubricants **10**, 277 (2022)
29. E.S. Ogunniran, R. Sadiku, S. Sinha Ray, Mater. Eng. **297**, 237 (2011)
30. D. Panaitescu, F. Ciuprina, M. Iorga, J. Appl. Polym. Sci. **122**, 1921 (2011)
31. K. Parvathi, M.T. Ramesan, J. Thermoplast. Compos. Mater. https://doi.org/10.1177/0892705722 1083495 (2022)

32. P. Maji, P.P. Pande, R.B. Choudhary, Bull. Mater. Sci. **38**, 417 (2015)
33. S.S. El-Khiyami, A.M. Ismail, R.S. Hafez, J. Inorg. Organomet. Polym. **31**, 4313 (2021)
34. B. Soman, S. Challagulla, S. Payra, S. Dinda, S. Roy, Res. Chem. Intermed. **44**, 2261 (2018)
35. M.T. Ramesan, T. Anilkumar, J. Chil. Chem Soc. **54**, 23 (2009)
36. K. Parvathi, B.K. Bahuleyan, M.T. Ramesan, J. Macromol. Sci. A **59**, 466 (2022)
37. Furhan, M.T. Ramesan, J. Appl. Polym. Sci. **139**, e52913 (2022)
38. F.S. Shokr, S.A. Al-Gahtany, J. Elastomers Plast. **46**, 470 (2013)
39. S. Oprea, V.A. Potolinca, J. Elastomers Plast. **50**, 276 (2017)
40. S. Karmakar, H.S. Mohanty, D. Behera, Eur. Phys. J. Plus. **136**, 1038 (2021)
41. S.P. Muduli, S. Parida, S. Nayak, Polym. Compos. **41**, 2855 (2020)
42. P. Nisha, S. Suresh, K. Jayamoorthy, Polym. Bull. **78**, 5255 (2021)
43. S.H. Wu, I. Masaharu, T. Natsuki, J. Reinf. Plast. Compos. **25**, 1957 (2006)
44. N.B.R. Kumar, V. Crasta, B.M. Praveen, Bull. Mater. Sci. **42**, 124 (2019)
45. S. Ha, Y. Choi, W. Lee, Compos. B. Eng. **224**, 109186 (2021)
46. K. Parvathi, B.K. Bahuleyan, M.T. Ramesan, J. Inorg. Organomet. Polym. **32**, 2827 (2022)
47. E. Guth, J. Appl. Phys. **16**, 20 (1945)
48. M. Mooney. J. Colloid Sci. 6162 (1951)
49. N. Adam, Nature **180**, 809 (1957)
50. A. Thabet, A.A. Ebnalwaled, Measurement **110**, 78 (2017)